Quantitative Susceptibility Mapping Displays Pallidofugal Fiber Tracts

Till Schneider[1], Andreas Deistung[2], Uta Biedermann[3], Sabine Heiland[1], Martin Bendszus[1], and Jürgen Reichenbach[2]
[1]*Neuroradiology, University of Heidelberg, Heidelberg, Germany,* [2]*Department of Medical Physics, University of Jena, Jena, Germany,* [3]*Department of Anatomy, University of Jena, Jena, Germany*

Target Audience: Scientists with interest in susceptibility weighted imaging, quantitative susceptibility mapping, and the depiction of smallest nerve fibers.

Introduction: The pallidofugal fiber tracts, an integral part of the comb system of Edinger [1], are difficult to visualize with T_1- and T_2-weigthed sequences and due to their very small caliber even diffusion tensor imaging (DTI) is not able to reliably depict them [2-4]. These fiber tracts, including the ansa lenticularis and the lenticular fasciculus, play an important role as a functional part of basal ganglionic neuronal networks [5,6]. Especially with regard to deep brain stimulation (DBS) surgery with electrode placement in the subthalamic nucleus (STN) identification of the pallidofugal fiber tracts is of clinical relevance as the positioning of the electrodes in relation to these tracts substantially influences outcome and side effects of the stimulation [7]. Therefore, the aim of the study was to investigate whether the pallidofugal pathways can be visualized on high resolution susceptibility weighted images (SWI), quantitative susceptibility maps (QSM), and maps of the effective transverse relaxation rate (R_2^*).

Material and Methods: *Data Acquisition:* Data were acquired on a 7T whole body scanner using a 3D gradient-echo sequence (TR/TE/FA/NEX=25ms/19.1ms/12°/1, GRAPPA with R=3) with isotropic resolution of 0.4 mm (2 subjects) and 0.6 mm (1 subject). To clarify whether the detected signal structures in the vicinity of the STN are not caused by veins, gradient-echo data were recorded of *(i)* a formalin-fixated brain of an 81-year-old male subject embedded in perfluoropolyether (Galden®, Solvay Inc., Thorofare, NJ, USA) (TE_{1-6} = 9ms/16ms/23ms/30ms/37ms/44ms, TR/FA/NEX=54ms/25°/NEX=3, voxel size = 0.28mm × 0.28mm × 0.28mm) and (*ii*) a healthy volunteer (25y) during inhalation of ambient air and carbogen (95% O_2, 5% CO_2) at 3T (TE_{1-4}=6.6ms/16.6ms/26.6ms/36.6ms, TR/FA/NEX=44ms/15°/1, voxel size = 0.65mm × 0.65mm × 0.65mm). *Data Processing*: SWI was computed by combining GRE magnitude and phase images using the standard procedure [8]. Magnetic susceptibility maps were computed based on GRE phase images by applying a 3D phase unwrapping algorithm, CNR-optimized combination of unwrapped multi-echo phase images, sophisticated harmonic artifact removal for phase data (SHARP) [9], and homogeneity enabled dipole inversion (HEIDI) [10] as described in [3]. Maps of the effective transverse relaxation were computed from multi-echo GRE data using logarithmic calculus. To display the course of the fiber tracts across several slices, the images are presented as mean intensity projections across 1.6 to 2 mm. *Data Analysis:* Magnetic susceptibility maps of the putative fiber tracts were quantitatively analyzed by manual identification using FSL (FMRIB, Oxford, UK).

Results: Tracts running from the globus pallidus to the subthalamic nucleus could be clearly depicted on SWI and QSM (see arrows in Fig.1). Interestingly, these tracts exhibit substantially increased magnetic susceptibility compared to the corticospinal (CST) tract. The susceptibility maps of a healthy subject during inhalation of ambient air and carbogen revealed similar susceptibilities of the pallidofugal fibers, while susceptibility in veins substantially decreased during carbogen breathing (Fig. 2). The susceptibility and R_2^* maps of a fixed human brain also displayed tracts originating in the globus pallidus, traversing the internal capsule and reaching the substantia nigra and the STN (Fig. 3). Susceptibility differences of the pallidofugal fiber tracts with respect to the CST ranged from 64.8 to 80.1 ppb, including the fibertracts studied post-mortem. The quantitative evaluation of the susceptibility differences between pallidofugal fibers and the CST in subjects aged from 18 to 81 years did not show an increase of paramagnetic behavior as seen with the basal ganglia in the course of aging [11].

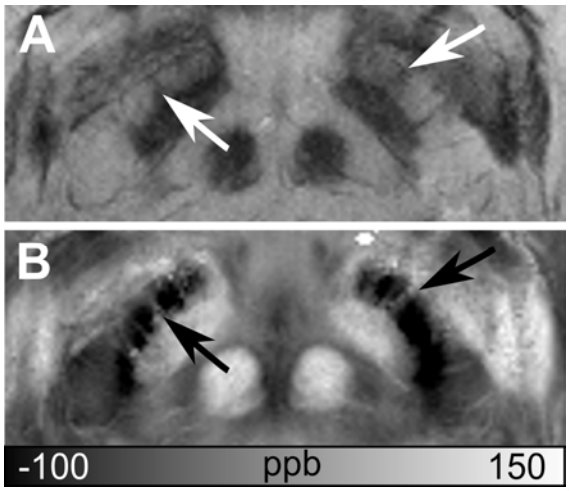

Figure 1: Susceptibility weighted image and magnetic susceptibility map of a 29 years old healthy subject showing the pallidofugal fiber tracts (*arrows*) are displayed in A and B, respectively.

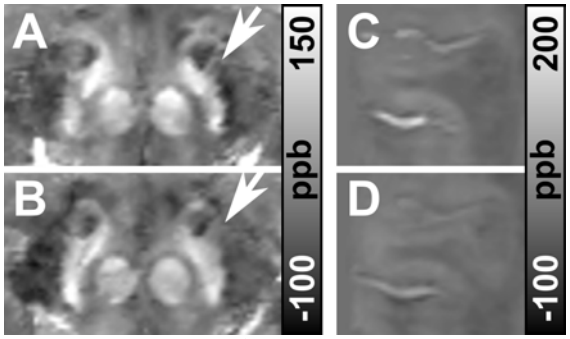

Figure 2: Susceptibility maps of a 25 year old subject during inhalation of ambient air (A,C) and carbogen (B,D) showing the midbrain (A,B) and cortical venous vessels (C,D).

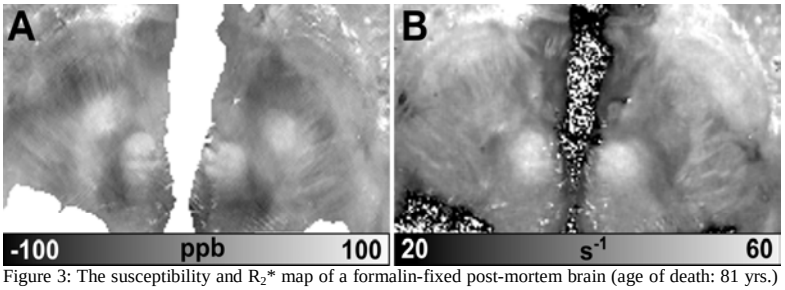

Figure 3: The susceptibility and R_2* map of a formalin-fixed post-mortem brain (age of death: 81 yrs.) are shown in A and B, respectively. The fibers are clearly discernible by high values of magnetic susceptibility and R_2*.

Discussion: We demonstrated that susceptibility based contrasts display pallidofugal fiber tracts. Analyzing MRI data acquired under different breathing conditions and from a bloodless fixed brain proved that the stripe-like pattern observed on susceptibility-based images was not caused by veins crossing the internal capsule but rather by fiber tracts running from the globus pallidus to enter the subthalamic nucleus. Since in conventional MRI examinations the pallidofugal fiber tracts are mainly oriented perpendicular to the static magnetic field ($\mathbf{B_0}$), while the corticospinal tracts traverse the brain nearly parallel to $\mathbf{B_0}$ depiction of the pallidofugal projections is also influenced by the orientation dependency of nerve fibers to $\mathbf{B_0}$. The difference between fibers running parallel and perpendicular to $\mathbf{B_0}$, determined to be $\Delta\chi$ = (22±8) ppb [12] and ΔR_2^* = 2.68 s^{-1} [12] at 3T, does not fully explain the observed severe paramagnetic behavior of the pallidofugal tracts. The presence of iron positive axons as well as iron positive granular oligodendrocytes in myelinated pallodofugal fiber bundles and especially in Edinger's comb system has been demonstrated histochemically [14,15]. Therefore, we propose that the encountered distinct paramagnetic behavior therefore is mainly caused by iron within pallidofugal tracts and to a lesser extent by orientation dependent effects of tissue microstructure.

Conclusion: Pallidofugal fiber tracts can be visualized non-invasively by employing susceptibility-based image contrasts. Considering the course of these tracts during stereotactic planning of DBS procedures could prove to reduce side effects and to improve beneficial effects of stimulation.

References:

[1] Nauta WJ, Mehler WR (1966) *Projections of the lentiform nucleus in the monkey.* Brain Res. [2] Van Camp N, et al. (2009) *Diffusion tensor imaging in a rat model of Parkinson's disease after lesioning of the nigrostriatal tract.* NMR Biomed. [3] Deistung A, et al. (2013) *High-Resolution MR Imaging of the Human Brainstem In vivo at 7 Tesla.* Front Hum Neurosci. [4] Soria G, et al. (2011) *Improved assessment of ex vivo brainstem neuroanatomy with high-resolution MRI and DTI at 7 Tesla*. Anat Rec (Hoboken).[5] Wilson CJ (2013) *Active decorrelation in the basal ganglia.* Neuroscience. [6] Carpenter MB, et. al.(1981) *Interconnections and organization of pallidal and subthalamic nucleus neurons in the monkey*. J Comp Neurol. [7] Herzog J. et al. (2007) *Stimulation of subthalamic fibre tracts reduces dyskinesias in STN-DBS.* Mov Disord. [8] Haacke EM et.al.(2004) *Susceptibility weighted imaging (SWI).* Magn Reson Med. [9] Schweser F et. al. (2011) *Quantitative imaging of intrinsic magnetic tissue properties using MRI signal phase: an approach to in vivo brain iron metabolism?* Neuroimage 54. [10] Schweser F, et. al. (2012) *Quantitative susceptibility mapping for investigating subtle susceptibility variations in the human brain.* Neuroimage 62. [11] Li W, et al. (2014) *Differential developmental trajectories of magnetic susceptibility in human brain gray and white matter over the lifespan.* Hum Brain Mapp [12]. Li W, et.al.(2012) *Magnetic susceptibility anisotropy of human brain in vivo and its molecular underpinnings.* Neuroimage. [13] Bender B, Klose U (2010) *The in vivo influence of white matter fiber orientation towards B(0) on T2* in the human brain.* NMR Biomed. [14] Morris CM et.al. (1992) *Histochemical distribution of non-haem iron in the human brain.* Acta Anat (Basel). [15] Hill JM, Switzer RC, 3rd (1984) *The regional distribution and cellular localization of iron in the rat brain.* Neuroscience.